

Atomistic simulations on ductile-brittle transition in $\langle 111 \rangle$ BCC Fe nanowires

G. Sainath^{1, a)} and B.K. Choudhary^{1, b)}

Deformation and Damage Modelling Section, Materials Development and Technology Division, Indira Gandhi Center for Atomic Research, HBNI, Kalpakkam, Tamilnadu -603102, India

Molecular dynamics simulations have been performed to understand the influence of temperature on the tensile deformation and fracture behavior of $\langle 111 \rangle$ BCC Fe nanowires. The simulations have been carried out at different temperatures in the range 10-1000 K employing a constant strain rate of $1 \times 10^8 \text{ s}^{-1}$. The results indicate that at low temperatures (10-375 K), the nanowires yield through the nucleation of a sharp crack and fails in brittle manner. On the other hand, nucleation of multiple $1/2\langle 111 \rangle$ dislocations at yielding followed by significant plastic deformation leading to ductile failure has been observed at high temperatures in the range 450-1000 K. At the intermediate temperature of 400 K, the nanowire yields through nucleation of crack associated with many mobile $1/2\langle 111 \rangle$ and immobile $\langle 100 \rangle$ dislocations at the crack tip and fails in ductile manner. The ductile-brittle transition observed in $\langle 111 \rangle$ BCC Fe nanowires is appropriately reflected in the stress-strain behavior and plastic strain at failure. The ductile-brittle transition increases with increasing nanowire size. The change in fracture behavior has been discussed in terms of the relative variations in yield and fracture stresses and change in slip behavior with respect to temperature. Further, the dislocation multiplication mechanism assisted by the kink nucleation from the nanowire surface observed at high temperatures has been presented.

Keywords: Molecular dynamics simulations, BCC Fe Nanowire, Plastic deformation, Ductile-Brittle transition

I. INTRODUCTION

In recent years, one dimensional metallic nanowires have attracted a considerable attention for research due to their unique properties and potential applications in future nano/micro electro-mechanical systems (NEMS/MEMS)¹. Due to the high surface area to volume ratio, the nanowires exhibit superior electrical, optical, and mechanical properties compared to their bulk counterparts. Particularly, BCC Fe nanowires, which possess good magnetic properties, find applications in data/memory storage devices, permanent magnets, spin electronics, magnetic field sensing, enhancement agents for magnetic resonance imaging (MRI), medical sensors, and other smart devices²⁻⁴. Improving the durability and reliability of these devices requires fundamental understanding of mechanical properties and associated deformation mechanisms. With detailed understanding of deformation and failure behavior, the mechanical properties of nanowires can be significantly improved by a suitable micro-structural design⁵. Further, the knowledge of deformation behavior also becomes important for fine-tuning the physical properties of nanowires with respect to reorientation, shape-memory, pseudo-elasticity, and super-plasticity.

Designing and performing mechanical testing of nanowires at different sample sizes, temperatures, and strain rates generally require sophisticated testing meth-

ods. In this context, molecular dynamics (MD) simulations are known to play a key role in exploring the deformation behavior of metallic nanowires. Based on detailed MD simulations, it has been shown that BCC Fe nanowires deform mainly either by the full dislocation slip or by the twinning mechanism. The deformation behavior of FCC and BCC nanowires has been reviewed in detail in Refs.⁶ and ⁷. Under tensile loading, BCC Fe nanowires oriented in $\langle 100 \rangle$, $\langle 112 \rangle$ and $\langle 102 \rangle$ axial directions deform predominantly by the twinning mechanism, whereas the full dislocation slip has been observed in $\langle 110 \rangle$ and $\langle 111 \rangle$ orientations⁸. Further, it has been shown that BCC Fe nanowires exhibit tension-compression asymmetry in deformation mechanisms^{8,9}. In contrast to tensile loading, the nanowire with $\langle 100 \rangle$ orientation deformed by the dislocation slip, whereas twinning was observed in $\langle 110 \rangle$ orientation under compressive loading⁸⁻¹⁰. Recently, Wang et al.¹¹ have provided the first experimental evidence of deformation twinning in BCC W nanowires with 15 nm diameter thereby conforming the predictions made using MD simulations. In addition to perfect nanowires, deformation by twinning is also observed in surface coated Fe¹² and Fe-Cr¹³ nanowires. It is interesting to note that when the BCC Fe nanowire deforms by the twinning mechanism, it has been found to undergo reorientation^{14,15} and exhibit the shape memory effect and pseudo-elasticity¹⁵⁻¹⁸. These mechanisms cannot be observed when the nanowires deform by the dislocation slip. The reorientation mechanism observed in BCC Fe nanowires exhibits a strong size and temperature dependence^{14,16}. It has been shown that the deformation by twinning leads to reorientation in nanowires

^{a)} Electronic mail: sg@igcar.gov.in

^{b)} Electronic mail: bkc@igcar.gov.in

of cross section width less than 11.42 nm. Beyond this size even though nanowires still deform by the twinning mechanism, the reorientation mechanism ceases to operate due to twin-twin interactions¹⁴. In addition to twinning, BCC Fe nanowires also exhibit peculiar dislocation behavior with respect to nanowire size, temperature, and strain rate. It has been shown that during early plastic deformation, dislocation loops initially consist of edge as well as screw components. However, with increasing strain, the edge components escape to the surface due to higher mobility and this leads to the accumulation of straight screw dislocations in $\langle 110 \rangle$ BCC Fe nanowires¹⁹. During compressive deformation of $\langle 100 \rangle$ BCC Fe nanowires, it has been shown that dislocation-mediated plasticity dominates at 500 K, whereas the twinning mechanism has been observed in addition to the dislocation slip at lower temperatures²⁰. A similar behavior has been observed with respect to temperature in $\langle 110 \rangle$ BCC Fe nanowires¹⁰.

Most of these studies in BCC metallic nanowires have been focused mainly on deformation aspects such as twinning and dislocation behavior⁸⁻²⁰. It is surprising that enough attention has not been paid towards the fracture behavior of BCC Fe nanowires. It is well known that BCC materials are generally difficult to deform at low temperatures leading to brittle fracture, whereas at high temperature, they fail by ductile manner. At nanoscale, the brittle to ductile transition with respect to temperature has been observed in semiconductor nanowires such as GaN²¹, ZnO²², and Si²³. Similar transition has also been reported in Cu nanowires with respect to size²⁴ and Ag nanowires with respect to the strain rate²⁵. It has been reported that the pre-cracked bulk single crystal BCC Fe oriented in the $\langle 100 \rangle / \{100\}$ direction exhibits brittle to ductile transition with increasing temperature²⁶. The temperature for brittle to ductile transition in the bulk BCC Fe single crystal has been found to vary in the range 130-154 K depending on the imposed strain rate. In addition to single crystal BCC Fe, Fe-9%Cr and Fe based ferritic steels also exhibit the brittle to ductile transition²⁷. In this context, it is important to examine whether there is a similar brittle to ductile transition in BCC Fe at nanoscale? In view of this, detailed MD simulations were performed on the tensile deformation of $\langle 111 \rangle$ BCC Fe nanowires at temperatures ranging from 10 to 1000 K in the present study. Emphasis has been given on the nature of defect nucleation with respect to temperature, the amount of plastic deformation before failure, and fracture behavior.

II. MD SIMULATION DETAILS

MD simulations have been performed in Large scale Atomic/Molecular Massively Parallel Simulator (LAMMPS) package²⁸ employing an embedded atom method (EAM) potential for BCC Fe given by Mendelev and co-workers²⁹. The important outcome of MD simu-

lations depends solely on the reliability of inter-atomic potential employed. It has been observed that some EAM potentials are reliable for many FCC systems, whereas for BCC systems, they may be less accurate in reproducing the defect structures, slip systems, twinning behavior, and phase transition. This difference in behavior with respect to the crystal structure results mainly from the non-planar core of screw dislocations in BCC systems, which makes the slip more complex compared to FCC systems. In the present investigation, the Mendelev EAM potential has been chosen mainly because several predictions made with this potential are in good agreement with either experimental observations or density functional theory (DFT) calculations. In agreement with DFT calculations³⁰, Mendelev EAM potential predicts a non-degenerate core structure for screw dislocations³¹. In contrast, all other potentials for BCC Fe predict a degenerate core structure. Similarly, depending on orientation, this potential correctly predicts deformation by twinning and dislocation slip in BCC Fe nanowires^{8,9,14,19,20}, which is quite close to the recent experimental observations in ultra-thin BCC W nanopillars¹¹. The mechanism of twin nucleation and growth^{14,32}, twin boundary as a dislocation source^{20,32}, twin migration stress^{14,33}, twist boundary structure³⁴, accumulation of straight screw dislocations¹⁹, and various twin-twin interactions^{32,33} are in good agreement with those observed experimentally^{33,35-37}.

BCC Fe nanowires of square cross-section width (d) = 8.5 nm and oriented in $\langle 111 \rangle$ axial direction with $\{110\}$ and $\{112\}$ side surfaces were created by generating atomic positions corresponding to the bulk Fe. Correspondingly, the simulation box contained about 110000 Fe atoms arranged in BCC lattice. The length (l) was twice the cross section width (d) of the nanowire. Periodic boundary conditions were chosen along the length direction, whereas the other two directions were kept free in order to mimic an infinitely long nanowire. After the initial construction of the nanowire, the energy minimization was performed by a conjugate gradient (CG) method to obtain a relaxed structure with equilibrium atomic positions corresponding to the nanowire. The minimization has been carried out until the energy change between two successive iterations divided by the initial energy is less than 10^{-6} . To put the sample at the required temperature, all the atoms have been assigned initial velocities according to the Gaussian distribution. Following this, the nanowire system was thermally equilibrated to a required temperature for 125 ps in canonical ensemble (constant NVT). The temperature is controlled with Nose-Hoover thermostat with a damping constant of 500 fs for all temperatures. This value of damping constant has ensured that the temperature fluctuations are always lower than 1% during simulation irrespective of test temperature. The velocity verlet algorithm has been used to integrate the equations of motion with a time step of 5 fs. In order to examine the influence of time step, the simulations have also been carried out with a lower time step

of 3 fs. It has been observed that there are no significant differences in the observed results.

Following thermal equilibration, the tensile deformation was performed at a constant strain rate of $1 \times 10^8 \text{ s}^{-1}$ along the axis of the nanowire. The strain rate considered here is higher than the typical experimental strain rates due to the inherent time-scale limitations in MD simulations. In order to reveal the brittle to ductile transition temperature, the atomistic simulations have been performed at different temperatures in the range 10 - 1000 K. The simulations at each temperature have been repeated five times, with a different random number seed for velocity distribution each time. The stress was calculated from the Virial definition of stress^{38,39} which takes the form

$$\sigma_{\alpha\beta} = \frac{1}{V} \left[\frac{1}{2} \sum_i^N \sum_{j \neq i}^N F_{ij}^\alpha r_{ij}^\beta - \sum_i^N m_i v_i^\alpha v_i^\beta \right]$$

where N is the total number of atoms, V is the volume of the nanowire or simulation cell, r_{ij} is the distance between atoms i and j , F_{ij} is the force between atoms i and j , m_i and v_i are the mass and velocity of particle i , and the indices α and β denote the Cartesian components. The first term in the above equation is due to the inter-atomic force and the second term is due to thermal vibrations, which becomes important with increasing temperature. The strain has been obtained as $(l - l_0)/l_0$, where l is the instantaneous length of the nanowire and l_0 is the initial length. The visualization of atomic configurations was performed using OVITO⁴⁰.

III. RESULTS

A. Stress-strain behavior

Figure 1 shows the stress-strain behavior of $\langle 111 \rangle$ BCC Fe nanowires at various temperatures ranging from 10 to 1000 K. It can be seen that all the nanowires undergo an elastic deformation and exhibit non-linear behavior at high strains. Further, during the elastic deformation at 10 and 50 K, a bump appears in the stress-strain curve at a strain value of 0.4-0.5. This bump may be due to weird behavior of surface atoms at low temperatures or it may arise from the inter-atomic potential. Following elastic deformation up to peak stress, yielding results in abrupt drop in flow stress in all the nanowires. The yield stress values have been obtained as the values of peak stress in the stress-strain curve. Following yielding, the $\langle 111 \rangle$ BCC Fe nanowires display two different behaviors during plastic deformation as shown for low (10-375 K) and high (400-1000 K) temperatures in Figs. 1(a) and 1(b), respectively. At low temperatures, the flow stress abruptly drops to zero indicating insignificant plastic deformation and sudden failure in the nanowires (Fig. 1(a)). On the other hand, the flow stress dropping

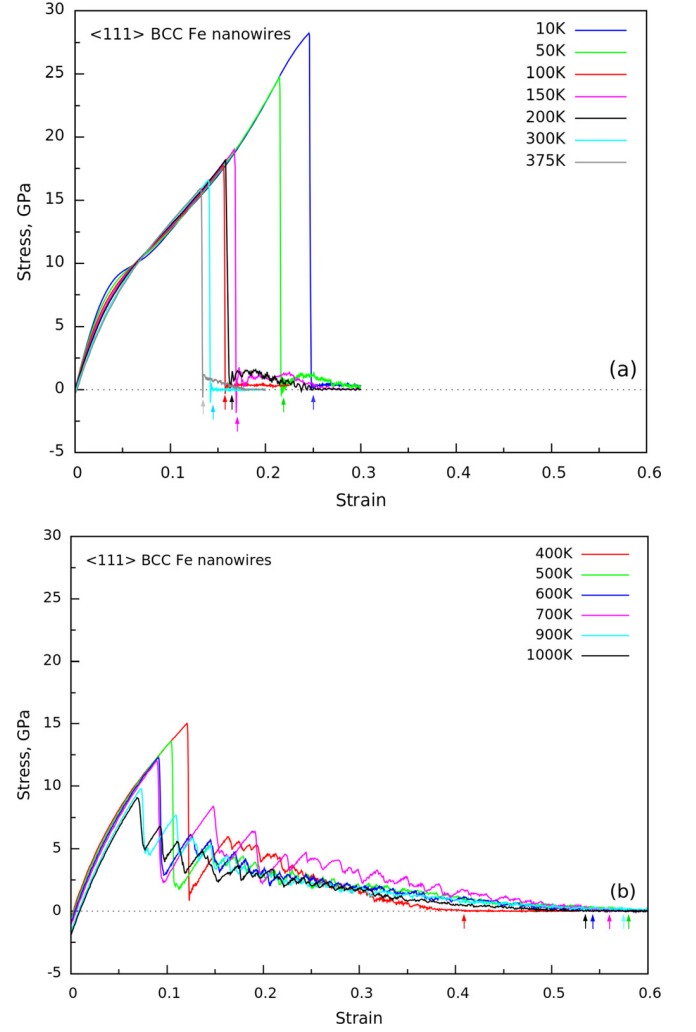


FIG. 1. Stress-strain behavior of $\langle 111 \rangle$ BCC Fe nanowires at (a) low (10-375 K) and (b) high (400-1000 K) temperatures. The failure locations have been marked by arrows. Since the loading in the present investigation is in the z -direction, the stress here refers to the z -component of the stress tensor, i.e., σ_{zz} .

to nonzero value followed by jerky flow and gradual decrease in flow stress during plastic deformation suggests ductile nature of nanowires at high temperatures (Fig. 1(b)).

The variations in Young's modulus, yield stress, and the accumulated plastic strain before failure as function of temperature are shown in Figs. 2(a)-2(c). In the presence of non-linear elastic deformation, the values of Young's modulus at different temperatures have been evaluated from the slope of initial linear elastic regime, that is, the slope of stress-strain curves for $\epsilon < 0.04$. Below this strain, the stress-strain curve is nearly linear for all temperatures. The non-linear portion at high elastic strains ($\epsilon > 0.04$) has been neglected for Young's modulus calculations. It can be seen that Young's modulus decreases rapidly up to 400 K followed by saturation at

higher temperatures (Fig. 2(a)). The variations in yield stress with respect to temperature exhibited a rapid decrease in yield stress up to 100 K followed by a gradual decrease with the increase in temperature (Fig. 2(b)). At about 100 K, a hump in yield stress or a concave down region can be seen in Fig. 2(b). Temperature (T) dependence of yield stress (σ_Y) obeying $\sigma_Y = A - B\sqrt{T}$ with $A = 26.8$ and $B = 0.58$ is superimposed as the broken line in Fig. 2(b). The yield stress values at all temperatures have been observed to be consistently lower than the theoretical strength of 27.6 GPa reported for $\langle 111 \rangle$ BCC Fe⁴¹. It is interesting to observe that apart from insignificant flow stress (Fig. 1(a)), the nanowires exhibit a negligible plastic strain during tensile deformation at low temperatures in the range 10-375 K (Fig. 2(c)). A significant increase in the accumulated plastic strain with the increase in temperature from 375 to 500 K can be seen in Fig. 2(c). Beyond 500 K, the plastic strain remains nearly constant. The accumulated plastic strain is obtained from stress-strain curves as total strain to failure minus elastic strain (the yield strain). The negligible amount of accumulated plastic strain obtained at lower temperatures arises from crack nucleation and growth till separation into two pieces. At higher temperatures, significant plastic deformation leading to failure results in higher values of accumulated plastic strain. From the variations in accumulated plastic strain before failure with temperature, it is clear that $\langle 111 \rangle$ BCC Fe nanowires undergo ductile-brittle transition with 400 K as a transition temperature.

B. Deformation and failure behavior

In order to understand the variations in stress-strain behavior, the atomic configurations have been analyzed using OVITO as a function of strain at different temperatures. Figure 3 shows the top view of nanowires during yielding at various temperatures. It can be seen that at low temperatures (10-375 K), yielding in the nanowires occurs mainly through the nucleation of a sharp crack with negligible dislocation activity at the crack tip. At transition temperature of 400 K, the nanowire yields primarily through the nucleation of crack associated with many mobile $1/2\langle 111 \rangle$ and immobile $\langle 100 \rangle$ dislocations in the vicinity of the crack. At temperatures higher than 400 K, the nanowires yielded only by the nucleation of multiple $1/2\langle 111 \rangle$ dislocations. In the temperature range 450-1000 K, no crack nucleation has been observed. The atomic snapshots as function of strain at 50 K representing deformation behavior of $\langle 111 \rangle$ BCC Fe nanowires at low temperatures is shown in Fig. 4. It can be seen that the crack nucleates from the corner of the nanowires without any dislocations at the tip (Fig. 4(a)) and grows rapidly along the direction at 45° angle with the loading axis (Figs. 4(b) and 4(c)). During crack growth, a few $1/2\langle 111 \rangle$ and $\langle 100 \rangle$ dislocations in the vicinity of crack tip can be seen in Figs. 4(b) and 4(c).

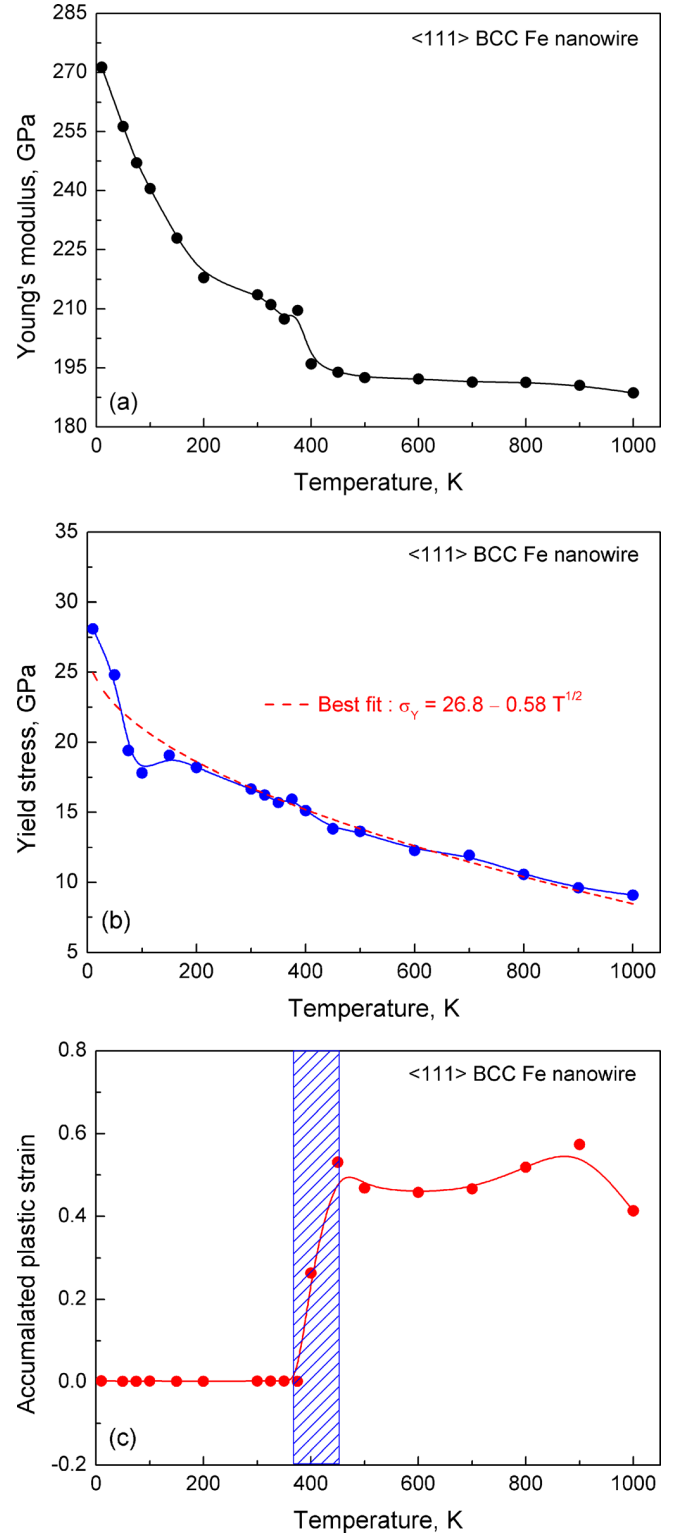


FIG. 2. Variations of (a) Young's modulus, (b) yield stress, and (c) accumulated plastic strain as a function of temperature for $\langle 111 \rangle$ BCC Fe nanowires. Temperature (T) dependence of yield stress (σ_Y) obeying $\sigma_Y = A - B\sqrt{T}$ with $A = 26.8$ and $B = 0.58$ is superimposed as the broken line in (b). The blue dashed region in (c) shows a ductile to brittle transition regime. The center of this regime has been taken as the transition temperature.

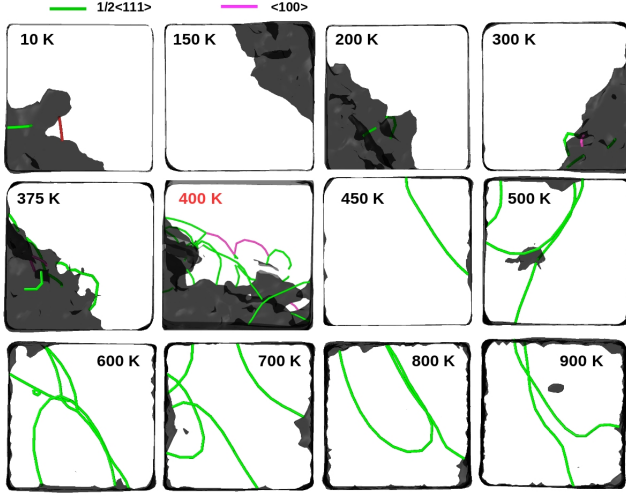


FIG. 3. Defect nucleation at yielding in $\langle 111 \rangle$ BCC Fe nanowires at different temperatures. The green lines indicate the dislocations with the Burgers vector $1/2\langle 111 \rangle$, the magenta lines represent the dislocations with the Burgers vector $\langle 100 \rangle$, and the dislocations with the unknown/unidentified Burgers vector are shown by red lines. The black regions indicate defective surfaces such as cracks.

The growing crack reaches the opposite surface within a short strain interval and the nanowire fails abruptly without showing any plastic deformation (Fig. 4). These observations clearly suggest that $\langle 111 \rangle$ BCC Fe nanowires fail in brittle manner in the temperature range 10-350 K and the peak stress in the stress-strain curves reflects the fracture strength of the nanowires. At 400 K, apart from yielding through nucleation of crack, several mobile $1/2\langle 111 \rangle$ and immobile $\langle 100 \rangle$ dislocations near crack tip have been observed (Fig. 3). With increasing deformation, the crack gets blunted by dislocation activity and as a result, the nanowire at 400 K exhibits considerable plastic deformation and fails in ductile manner at high strains.

Contrary to crack nucleation at low temperatures, the nanowires yield through the nucleation of multiple $1/2\langle 111 \rangle$ dislocations at high temperatures in the range 450-1000 K (Fig. 3). Therefore, the peak stresses in the stress-strain curves at high temperatures necessarily indicate stress for the nucleation of dislocations in an otherwise perfect nanowire. At high temperatures, yielding through dislocation nucleation followed by plastic deformation results in flow stress drop to non-zero values (Fig. 1(b)). The atomic configurations representing typical yielding and plastic deformation of nanowires at high temperatures (450-1000 K) are shown for 700 K in Fig. 5. The yielding by the nucleation of dislocations from the nanowire corner can be seen in Fig. 5(a). It can also be seen that the dislocations nucleated from the corners glide with the increase in plastic deformation on their respective glide planes (mainly $\{110\}$ type) and eventually escape to the surface (Figs. 5(b) and 5(c)). The continuous nucleation and glide of dislocations on interacting

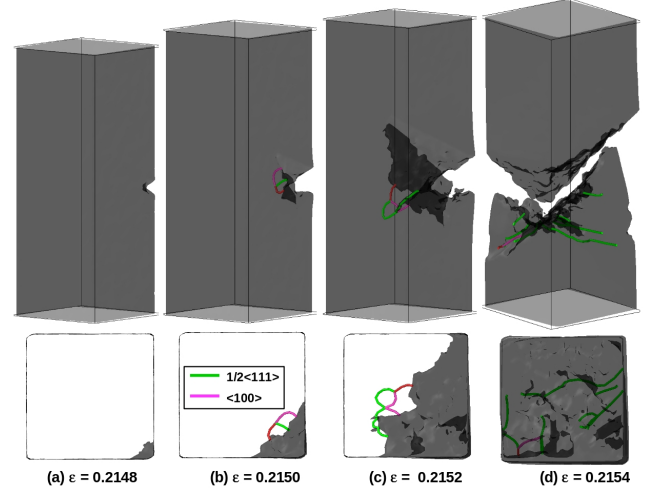


FIG. 4. Atomic snapshots as a function of total strain at 50 K representing deformation behavior of $\langle 111 \rangle$ Fe nanowires at low temperatures in the range 10-375 K. The color code details are described in Fig. 3 caption.

glide planes leads to the formation of well defined necking (Fig. 5(d)) and the nanowires fail in ductile manner at significantly higher plastic strains. Interestingly at high temperatures of 900 and 1000 K, it has been observed that the disordered atoms in the neck region rearrange themselves and forms the pentagonal atomic chain as shown in Fig. 6. The atomic chain consists of a central atom sandwiched between the two pentagonal rings, where each pentagonal ring consists of 5 atoms. Formation of pentagonal atomic chains has been reported in $\langle 100 \rangle$ BCC Fe and Fe-Cr nanowires at high temperatures for ultra thin cross-section width less than 2.83 nm^{13,42}. The transformation of perfect BCC lattice into the pentagonal structure has been described in terms of energy minimization^{42,43}.

C. Dislocation multiplication mechanism and dissociation of immobile dislocation

In bulk materials, the dislocations generally multiply by the well known Frank-Read mechanism. However, the Frank-read mechanism no longer operates when the size is reduced to nanoscale. A special dislocation multiplication mechanism operating during plastic deformation of $\langle 111 \rangle$ BCC Fe nanowires at high temperatures (450-1000 K) is shown in Fig. 7. It can be seen that when a mixed dislocation nucleates from the nanowire corner (Fig. 7(a)), it align itself to a straight screw configuration with further glide (Fig. 7(b)). This straight screw dislocation glides through the kink-pair mechanism, where the kinks nucleate from the nanowire surfaces. When the kinks having different orientations nucleated from two different surfaces move towards each other, a cusp develops at their intersection point on the straight screw

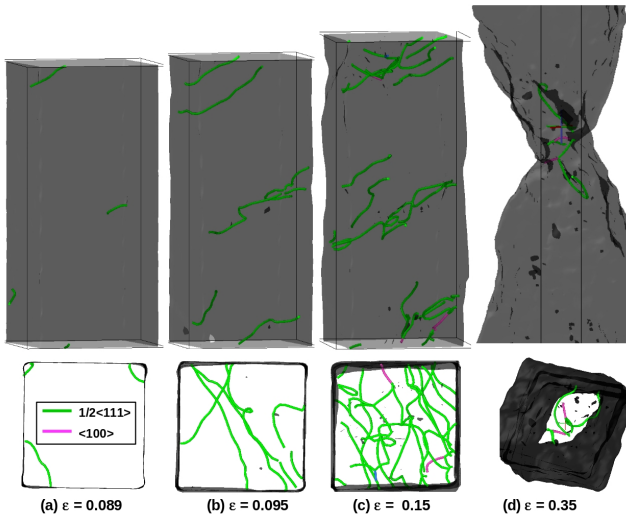


FIG. 5. Atomic snapshots as a function of total strain at 700 K representing deformation behavior of $\langle 111 \rangle$ Fe nanowires at high temperatures in the range 450-1000 K. The color code details are described in Fig. 3 caption.

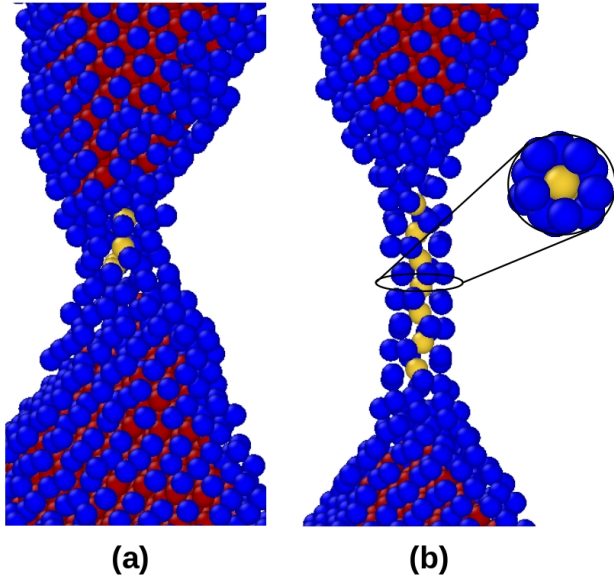


FIG. 6. Formation of pentagonal atomic chain in the necking region during deformation of $\langle 111 \rangle$ Fe nanowires at 900 K. The red color represents perfect BCC atoms, blue color indicates the atoms in the non-crystalline structure, and yellow indicates the atoms in five fold symmetry.

dislocation (Figs. 7(b) and 7(c)). With increasing deformation, the radius of curvature of the cusp decreases (as observed from the nanowire axial direction, i.e., top view) and it appears like a dislocation loop as shown in Fig. 7(c). As the loop grows with strain, the edge component of the loop reaches the nearby nanowire surface and this creates three independent screw dislocations in the nanowire (Figs. 7(d) and 7(e)). The mechanism of

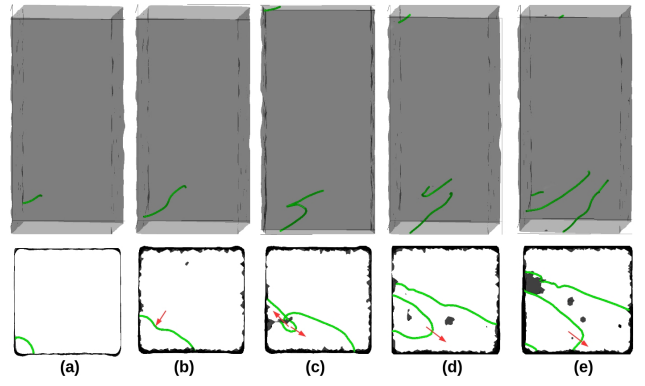


FIG. 7. A special dislocation multiplication mechanism observed in $\langle 111 \rangle$ Fe nanowires at high temperatures in the range 450-1000 K. The color code details are described in Fig. 3 caption.

kink nucleation and glide from the nanowire surface resulting in dislocation multiplication into three independent dislocations has been shown in Mo nanopillars by Weinberger and Cai⁴⁴ using a combination of MD and dislocation dynamics simulations. It has been suggested that a similar dislocation multiplication will be operating in other BCC nanowires⁶ as observed in the present study. This observation further supports the applicability of Mendelev EAM potential for understanding deformation behavior in BCC Fe nanowires. For the operation of this special dislocation multiplication mechanism, Lee et al.⁴⁵ laid down necessary conditions on the mobility of edge and screw dislocations. Using dislocation dynamics simulations, it has been shown that the surface controlled dislocation multiplication occurs only when the screw dislocation mobility is much lower than that of edge dislocation⁴⁵. When the mobility of edge and screw dislocations is equal, the complete dislocation gets annihilated at the surface and the dislocation multiplication does not occur⁴⁵.

It has been observed that the deformation behavior of $\langle 111 \rangle$ BCC Fe nanowires is dominated by the slip of $1/2\langle 111 \rangle$ mobile dislocations at high temperatures (450-1000 K). In addition to $1/2\langle 111 \rangle$ dislocations, $\langle 100 \rangle$ immobile dislocations have also been observed. The different stages of the formation and dissociation of $\langle 100 \rangle$ immobile dislocation emanating from the interactions of two $1/2\langle 111 \rangle$ mobile dislocations are shown in Fig. 8. Initially, two $1/2\langle 111 \rangle$ dislocations nucleate from the nanowire surface and attract towards each other (Fig. 8(a)). With increasing strain, part of these two dislocations combine and form a $\langle 100 \rangle$ immobile dislocation (Fig. 8(b)). Subsequent glide of these mobile dislocations at Y-junction leads to a zipping process, which increases the length of the immobile dislocation (Figs. 8(c) and 8(d)). Following completion of zipping process, long $\langle 100 \rangle$ immobile dislocation is obtained (Figs. 8(e) and 8(f)). The formation of $\langle 100 \rangle$ dislocation has also been observed during the compressive de-

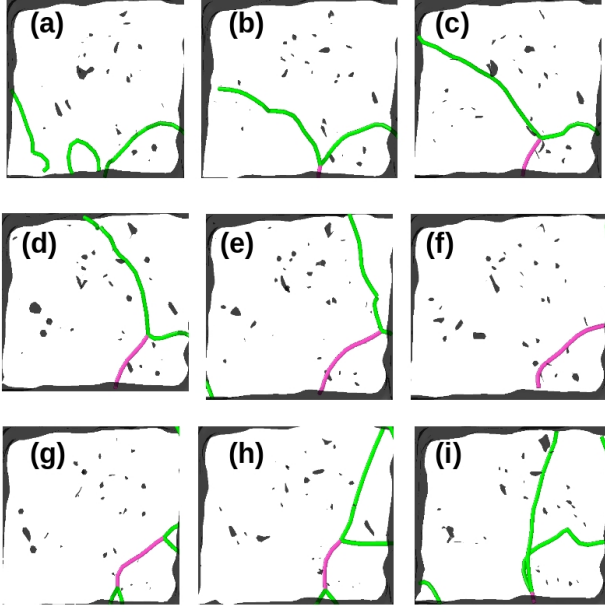


FIG. 8. Surface assisted formation and dissociation of $\langle 100 \rangle$ immobile dislocations through two $1/2\langle 111 \rangle$ mobile dislocations at high temperatures. The color code details are described in Fig. 3 caption.

formation of $\langle 100 \rangle$ BCC Fe nanopillars²⁰. Generally, it is assumed that $\langle 100 \rangle$ dislocation is highly stable and immobile and aids in the nucleation of micro-cracks in BCC metals. Contrary to this, it has been observed in the present study that $\langle 100 \rangle$ dislocation is not stable during the deformation of nanowires and dissociates into two mobile dislocations with Burgers vector $1/2\langle 111 \rangle$ as shown in Figs. 8(g)-8(i). The dissociation/unzipping process of $\langle 100 \rangle$ dislocations initiates from the surface of the nanowire through the formation of two Y-junctions (Fig. 8(g)) and with increasing deformation, one of the Y-junction penetrates towards the other end of the dislocation (Figs. 8(h) and 8(i)). According to Franks criterion, the dissociation of $\langle 100 \rangle$ dislocation is difficult to be observed as this reaction leads to the increase in energy (i.e., $b_1^2 < b_2^2 + b_3^2$, where b_1 is the Burgers vector of immobile dislocation and b_2 and b_3 are the Burgers vector of dissociated dislocations). However, this dislocation reaction becomes feasible at high energy or stresses in the order of GPa as observed in the present study. Since the nanowire surfaces can act as local stress raisers, it is reasonable to conclude that the surfaces of the nanowires/nanopillars provide a source for the dissociation of immobile dislocations in BCC nanowires. The dissociation of $\langle 100 \rangle$ screw dislocation has also been observed at the twist boundary of BCC Fe and it has been shown that the surfaces aid to the dissociation³⁴.

IV. DISCUSSION

A. Temperature dependence of yield stress

In BCC/FCC metallic nanowires, the variations in yield stress (σ_Y) with temperature (T) follow either $\sigma_Y = A - BT$ or $\sigma_Y = A - B\sqrt{T}$ relation depending upon the inter-atomic potential used in MD simulations^{6,46}. In BCC Fe nanowires, it has been shown that the yield stress follows $\sigma_Y = A - B\sqrt{T}$ relation with Mendelev EAM potential⁴⁷. In agreement with above observation, the observed decrease in yield stress with the increase in temperature in the present study followed the relation $\sigma_Y = 26.8 - 0.58\sqrt{T}$. It can be seen that the observed temperature dependence of yield stress in BCC Fe nanowires (Fig. 2(b)) is different from their bulk single crystal counterparts. In bulk single crystals, the yield stress generally saturates above a critical temperature⁴⁸⁻⁵¹. In BCC Fe nanowires, saturation in yield stress has not been observed. This difference in behavior essentially arises from the difference in yielding events in BCC Fe nanowires and bulk single crystals⁴⁷. In nanowires, yielding results from the nucleation of defects, whereas movement of existing dislocations leads to yielding in the bulk single crystals. The presence of a hump or concave down region in the yield stress - temperature curve at about 100 K (Fig. 2(b)) is in agreement with the experimental observations reported for the pure bulk single crystal of BCC Fe⁴⁸⁻⁵¹. However, the occurrence of hump in the bulk single crystal has been observed in the temperature range 200-250 K. Further, it has been shown that this hump disappears in Fe specimens doped with a small amount of carbon atoms^{48,49}. These studies indicate that the hump is intrinsic to pure BCC Fe lattice. Guyot and Dorn⁵² have suggested that this hump in flow stress is due to the double hump shape of Peierls potential in BCC lattice. Interestingly, the Mendelev EAM potential also shows the double hump Peierls potential for BCC Fe⁵³. Therefore, the hump in yield stress versus temperature curve observed in the present investigation can be attributed to the double hump shape of the Peierls potential.

B. Ductile-brittle transition

Influence of temperature on tensile deformation of $\langle 111 \rangle$ BCC Fe nanowire clearly indicated that the nanowires yield through the nucleation of a sharp cracks and fail in brittle manner at low temperatures (10-375 K), whereas nucleation of multiple dislocations at yielding followed by significant plastic deformation leads to ductile failure at high temperatures (450-1000 K). At 400 K, the nanowire yielded by crack nucleation and reasonable dislocation activity at the crack tip resulted in ductile failure. The above failure behavior with respect to temperature is also reflected in the tensile ductility. BCC Fe nanowires displayed negligible plastic strain

at low temperatures (10-375 K) followed by a rapid increase in the accumulated plastic strain in the temperature range 375-500 K and high but nearly constant plastic strain above 500 K. These observations clearly suggest that BCC Fe nanowires display ductile-brittle transition at 400 K. Similar ductile-brittle transition has been observed in bulk single crystal BCC Fe²⁶. However, the transition temperature of 400 K observed in nanowires is significantly higher than 130 K reported for the strain rate $4.46 \times 10^{-5} \text{ s}^{-1}$ in bulk single crystal BCC Fe²⁶. An increase in transition temperature to 154 K with the increase in strain rate to $4.46 \times 10^{-3} \text{ s}^{-1}$ has also been reported for bulk single crystal BCC Fe²⁶. Based on the detailed investigation, the ductile to brittle transition in BCC Fe has been successfully modeled as a function of strain rate^{5,4}. A transition temperature of 320 K has been predicted for the strain rate $1 \times 10^3 \text{ s}^{-1}$ in BCC Fe^{5,4}. In order to examine the strain rate dependence of ductile-brittle transition in Fe nanowires, MD simulations have also been carried out at a strain rate of $1 \times 10^9 \text{ s}^{-1}$. A transition temperature of 450 K observed for $1 \times 10^9 \text{ s}^{-1}$ clearly indicates that the ductile-brittle transition temperature (DBTT) increases with increasing strain rate in the Fe nanowire. However, further studies are needed in this direction. The higher transition temperatures than the bulk counterparts observed in the present investigation can be ascribed as a consequence of high strain rates used in MD simulations.

The brittle to ductile transition behavior can be explained based on the relative variations of yield and fracture stresses with respect to temperature. It is known that Youngs modulus (E) is related to the perfect or fracture strength σ_f of a material through the relation $\sigma_f = (E\gamma_s/a_0)^{1/2}$, where γ_s is surface energy of the fractured surfaces and a_0 is interatomic spacing⁵⁵. By making a reasonable approximation of $\gamma_s = Ea_0/20$, a rough estimate of strength in terms of Youngs modulus shows that σ_f varies between $E/4$ and $E/15$ depending on material and test conditions⁵⁵. The variations of yield strength and σ_f (obtained by $E/10$, $E/13$, and $E/15$) as a function of temperature are shown in Fig. 9. It can be clearly seen that σ_f is less sensitive to temperature compared to yield stress and as a result, all the three σ_f curves cross over yield strength at different temperatures. The temperatures of cross-over for $E/10$, $E/13$, and $E/15$ have been obtained as 40 K, 400 K, and 570 K, respectively. The temperature at which the fracture stress crosses the yield strength is considered as brittle-ductile transition temperature. Below the transition temperature, the fracture stress is either lower or close to yield stress and this leads to fracture before yielding. Above the transition temperature, fracture stress is much higher than the yield stress and this result in yielding, significant plastic deformation, and ductile failure. From the above comparison, it is clear that σ_f values evaluated as $E/13$ crosses the yield strength at 400 K as observed in the MD simulations. Therefore, $\sigma_f = E/13$ can be assumed to represent the brittle to ductile transition behavior of

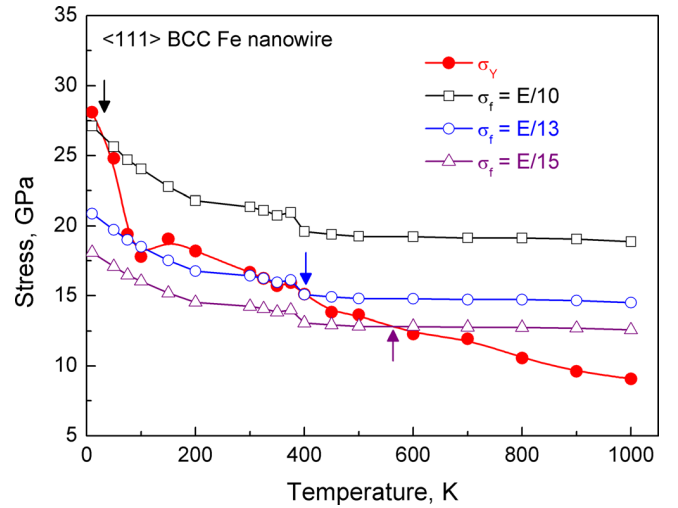


FIG. 9. Variations of yield stress as a function of temperature along with fracture stresses (σ_f) approximated to $E/10$, $E/13$, and $E/15$.

<111> BCC Fe nanowire.

In a single phase BCC Fe-Co alloy, Johnston et al.⁵⁶ have shown that the change in fracture behavior is primarily associated with a change in slip behavior and the yield stress plays a secondary role. In the BCC Fe-Co alloy, it has been shown that when the deformation is restricted to a planar glide, the alloy failed in brittle manner, whereas the wavy glide induces the ductile behavior⁵⁶. This correlation has been ascribed to the requirement of at least five independent slip systems to induce a small and homogeneous strain, that is, von-Mises criterion. In the present study, it has been observed that when the nanowires failed in brittle manner, a few dislocations present at the crack tip have been associated with only one or two independent slip systems (Figure 4). On the other hand, when the nanowires show ductile behavior, the wavy glide is extensively observed as depicted in Figs. 5 and 7. In the case of wavy glide, the requirement of five independent slip systems is naturally met and this induces significant plastic deformation leading to ductile fracture. It is important to mention that the ductile-brittle transition observed in the <111> BCC Fe nanowire in the present study is absent in <100> and <110> orientations of BCC Fe^{14,19}. It has been observed that the BCC Fe nanowires with <100> and <110> orientations undergo significant plastic deformation and fails via ductile mode even at the lowest temperature of 10 K^{14,19}. The activation of multiple slip systems satisfying the von-Mises criterion even at 10 K in <110> BCC Fe nanowires lead to gross plastic deformation and high ductility¹⁹. In <100> BCC Fe nanowire, different deformation mechanisms of twinning and reorientation at 10 K results in high ductility¹⁴. Apart from orientation, the nanowire size and shape also play an important role on the deformation mechanisms. In order to reveal the influence of size on the observed ductile-brittle transition,

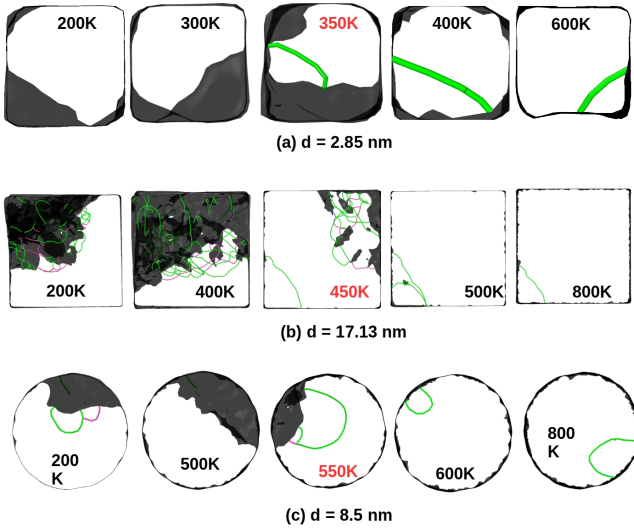


FIG. 10. Defect nucleation in square cross-section nanowires of (a) low and (b) high size with respect to temperature. Defect nucleation in the circular cross-section nanowire of $d = 8.5$ nm with respect to temperature is shown in (c). The ductile-brittle transition temperature in each case has been highlighted in the red color. The color code details are described in Fig. 3 caption.

further MD simulations have been carried out on two different nanowire sizes of 2.85 and 17.13 nm representing lower and higher sizes, respectively. The results indicate that the ductile-brittle transition temperature increases with increasing nanowire size. For the nanowire of cross-section width (d) = 2.85 nm, the transition has been observed at 350 K (Fig. 10(a)), whereas for nanowires with $d = 17.13$ nm, it has been observed at 450 K (Fig. 10 (b)). Similarly, the simulations performed with the circular cross-section nanowire of 8.5 nm diameter yields a transition temperature of 550 K (Fig. 10(c)), which is higher than that observed for the square cross-section nanowire. These results also indicate that the circular cross-section nanowires attains higher yield strength values, and as a result, the yield stress versus temperature curve in Fig. 9 crosses the fracture stress versus temperature curve at relatively higher temperature compared to the square cross-section nanowire.

V. CONCLUSIONS

The temperature dependent deformation and failure behavior of $\langle 111 \rangle$ BCC Fe nanowires has been investigated by molecular dynamics simulations. The simulation results indicate that $\langle 111 \rangle$ BCC Fe nanowires undergo ductile-brittle transition at 400 K. Below this temperature, the nanowires yield through the nucleation of a sharp crack and fails in a brittle manner, whereas at high temperatures, the nucleation of multiple $1/2\langle 111 \rangle$ dislocations associated with significant plastic

deformation leads to ductile failure. The ductile-brittle transition in $\langle 111 \rangle$ BCC Fe nanowires results from the relative variations of yield and fracture stresses as well as slip behavior with respect to temperature. Above the transition temperature of 400 K, the lower yield stress than the fracture stress facilitates yielding by the nucleation of dislocations and significant plastic deformation before ductile failure. This is well supported by the occurrence of wavy glide and dislocation multiplications at high temperatures. Below the transition temperature, the lower fracture stress than the yield stress leads to the yielding by crack nucleation and brittle failure with negligible dislocation activity in the nanowires. Further, it has been observed that the nanowire surfaces aid in dislocation multiplication mechanism and also in dissociation of immobile dislocations.

- ¹C.M. Lieber, MRS Bull. 28 (2003) 486.
- ²American elements, Iron Nanorods. <http://www.americanelements.com/femnr.html>.
- ³J.I. Martina, J. Nogues, K. Liu, J.L. Vicent, I.K. Schuller, J. Magn. Mater. 256 (2003) 449.
- ⁴X.Y. Zhang, G.H. Wen, Y.F. Chan, R.K. Zheng, X.X. Zhang, N. Wang, Appl. Phys. Lett. 83 (2003) 3341.
- ⁵J. Wang¹, F. Sansoz, J. Huang, Y. Liu, S. Sun, Z. Zhang, S.X. Ma, Nat. Commun. 4 (2013) 1742.
- ⁶C.R. Weinberger, W. Cai, J. Mater. Chem. 22 (2011) 3277.
- ⁷C.R. Weinberger, B.L. Boyce, and C.C. Battaile, Int. Mater. Rev. 58 (2013) 296.
- ⁸G. Sainath, B.K. Choudhary, Comput. Mater. Sci. 111 (2016) 406.
- ⁹C.J. Healy, G.J. Ackland, Acta Mater. 70 (2014) 105.
- ¹⁰A.B. Hagen, B.D. Snartland, and C. Thaulow, Acta Mater. 129 (2017) 398.
- ¹¹J. Wang, Z. Zeng, C.R. Weinberger, Z. Zhang, T. Zhu, S.X. Mao, Nat. Mater. 14 (2015) 594.
- ¹²G. Aral, Y.-J. Wang, S. Ogata, A.C.T. van Duin, J. Appl. Phys. 120 (2016) 135104.
- ¹³J. Byggmatar, F. Granberg, A. Kuronen, K. Nordlund, K.O.E. Henriksson, J. Appl. Phys. 117 (2015) 014313.
- ¹⁴G. Sainath, B.K. Choudhary, and T. Jayakumar, Comput. Mater. Sci. 104 (2015) 76.
- ¹⁵J. Zhu and D. Shi, J. Phys. D: Appl. Phys. 44 (2011) 055404.
- ¹⁶A. Cao, J. Appl. Phys. 108 (2010) 113531.
- ¹⁷S. Li, X. Ding, J. Deng, T. Lookman, J. Li, X. Ren, J. Sun, A. Saxena, Phys. Rev. B 82 (2010) 205435.
- ¹⁸Y. Yang, S. Li, X. Ding, J. Sun, E.K.H. Salje, Adv. Funct. Mater. 26 (2016) 760.
- ¹⁹G. Sainath, B.K. Choudhary, Mater. Scie. Eng. A 640 (2015) 98.
- ²⁰A. Dutta, Acta Mater. 125 (2017) 219.
- ²¹Z. Wang, X. Zu, F. Gao, W.J. Weber, Appl. Phys. Lett. 89 (2006) 243123.
- ²²Z. Yuan, K. Nomura, A. Nakano, Appl. Phys. Lett. 100 (2012) 153116.
- ²³F.A. El Nabi, J. Godet, S. Brochard, L. Pizzagalli, Modell. Simul. Mater. Sci. Eng. 23 (2015) 025010.
- ²⁴C. Peng, Y. Zhan, J. Lou, Small 8 (2012) 1889.
- ²⁵R. Ramachandramoorthy, W. Gao, R. Bernal, H. Espinosa, Nano Lett. 16 (2016) 255.
- ²⁶M. Tanaka, E. Tarleton, S.G. Roberts, Acta Mater. 56 (2008) 5123.
- ²⁷T.D. Joseph, M. Tanaka, A.J. Wilkinson, S.G. Roberts, J. Nucl. Mater. 367-370 (2007) 637.
- ²⁸S.J. Plimpton, J. Comput. Phys. 117 (1995) 1.
- ²⁹M.I. Mendelev, S. Han, D.J. Srolovitz, G.J. Ackland, D.Y. Sun, M. Asta, Philos.Mag. 83 (2003) 3977.

- ³⁰S.L. Frederiksen, K.W. Jacobsen, *Philos. Mag.* 83 (2003) 365.
- ³¹J. Chaussidon, M. Fivel, and D. Rodney, *Acta Mater.* 54 (2006) 3407.
- ³²G. Sainath, B.K. Choudhary, *Philos. Mag.* 96 (2016) 3502.
- ³³A. Ojha, H. Sehitoglu, L. Patriarca, and H.J. Maier, *Philos. Mag.* 94 (2014) 1816.
- ³⁴G. Sainath, B.K. Choudhary, *Phil. Mag. Lett.* 96 (2016) 469.
- ³⁵H.W. Paxton, *Acta Metall.* 1 (1953) 141.
- ³⁶D. Hull, *Acta Metall.* 9 (1961) 909.
- ³⁷S.M. Ohr, D. N. Beshers, *Philos. Mag.* 8 (1963) 1343.
- ³⁸K. S. Cheung and S. Yip, *J. Appl. Phys.* 70 (1991) 5688.
- ³⁹M. Zhou, *Proc. R. Soc. London, Ser. A* 459 (2003) 2347.
- ⁴⁰A. Stukowski, *Modelling Simul, Mater. Sci. Eng.* 18 (2010) 015012.
- ⁴¹M. Friak, M. Sob, V. Vitek, *Philos. Mag.* 83 (2003) 3529.
- ⁴²G. Sainath, B.K. Choudhary, *Mater. Res. Express* 3 (2016) 125022.
- ⁴³O. Gulseren, F. Ercolessi, and E. Tosatti, *Phys. Rev. Lett.* 80 (1998) 3775.
- ⁴⁴C.R. Weinberger, W. Cai, *Proc. Nat. Acad. Sci.* 105 (2008) 14304.
- ⁴⁵S.W. Lee, Y.T. Cheng, I. Ryu, J.R. Greer, *Sci. China Tech. Sci.* 57 (2014) 652.
- ⁴⁶E. Rabkin, H.S. Nam, D. J. Srolovitz, *Acta Mater.* 55 (2017) 2085.
- ⁴⁷S. Kotrechko, A. Ovsjannikov, *Philos. Mag.* 89 (2009) 3049.
- ⁴⁸D.J. Quesnel, A. Sato, M. Meshii, *Mater. Sci. Eng.* 18 (1975) 199.
- ⁴⁹J. Diehl, M. Schreiner, S. Staiger and S. Zwiesele, *Scr. Metall.* 10 (1976) 949.
- ⁵⁰D. Tseng, K. Tangri, *Scr. Metall.* 11 (1977) 719.
- ⁵¹E. Kuramoto, Y. Aono, K. Kitajima, *Scr. Metall.* 13 (1979) 1039.
- ⁵²P. Guyot, J. E. Dorn, *Can. J. Phys.* 45 (1967) 983.
- ⁵³L. Ventelon, F. Willaime, E. Clouet, and D. Rodney, *Acta Mater.* 61 (2013) 3973.
- ⁵⁴K.K. Kashinath, Modeling of brittle to ductile transition in BCC metals : strain rate and temperature dependence in alpha - iron and tantalum monocrystals, M.S Thesis, University of California, San Diego, (2013) p. 85.
- ⁵⁵G.E. Dieter, *Mechanical Metallurgy*. 3rd. Ed. McGraw Hill, NewYork (1986) p. 245.
- ⁵⁶T.L. Johnston, G. Davies, N.S. Stoloff, *Philos. Mag.* 12 (1965) 305.